NASA/TM-20230003935

# High-Temperature Solid Particle Erosion Behavior of an Environmental Barrier Coating

*Michael J. Presby*
*Glenn Research Center, Cleveland, Ohio*

June 2023

# NASA STI Program . . . in Profile

Since its founding, NASA has been dedicated to the advancement of aeronautics and space science. The NASA Scientific and Technical Information (STI) Program plays a key part in helping NASA maintain this important role.

The NASA STI Program operates under the auspices of the Agency Chief Information Officer. It collects, organizes, provides for archiving, and disseminates NASA's STI. The NASA STI Program provides access to the NASA Technical Report Server—Registered (NTRS Reg) and NASA Technical Report Server—Public (NTRS) thus providing one of the largest collections of aeronautical and space science STI in the world. Results are published in both non-NASA channels and by NASA in the NASA STI Report Series, which includes the following report types:

- TECHNICAL PUBLICATION. Reports of completed research or a major significant phase of research that present the results of NASA programs and include extensive data or theoretical analysis. Includes compilations of significant scientific and technical data and information deemed to be of continuing reference value. NASA counter-part of peer-reviewed formal professional papers, but has less stringent limitations on manuscript length and extent of graphic presentations.

- TECHNICAL MEMORANDUM. Scientific and technical findings that are preliminary or of specialized interest, e.g., "quick-release" reports, working papers, and bibliographies that contain minimal annotation. Does not contain extensive analysis.

- CONTRACTOR REPORT. Scientific and technical findings by NASA-sponsored contractors and grantees.

- CONFERENCE PUBLICATION. Collected papers from scientific and technical conferences, symposia, seminars, or other meetings sponsored or co-sponsored by NASA.

- SPECIAL PUBLICATION. Scientific, technical, or historical information from NASA programs, projects, and missions, often concerned with subjects having substantial public interest.

- TECHNICAL TRANSLATION. English-language translations of foreign scientific and technical material pertinent to NASA's mission.

For more information about the NASA STI program, see the following:

- Access the NASA STI program home page at http://www.sti.nasa.gov

- E-mail your question to help@sti.nasa.gov

- Fax your question to the NASA STI Information Desk at 757-864-6500

- Telephone the NASA STI Information Desk at 757-864-9658

- Write to:
  NASA STI Program
  Mail Stop 148
  NASA Langley Research Center
  Hampton, VA 23681-2199

NASA/TM-20230003935

# High-Temperature Solid Particle Erosion Behavior of an Environmental Barrier Coating

*Michael J. Presby*
*Glenn Research Center, Cleveland, Ohio*

National Aeronautics and
Space Administration

Glenn Research Center
Cleveland, Ohio 44135

June 2023

This report is a formal draft or working paper, intended to solicit comments and ideas from a technical peer group.

This work was sponsored by the Advanced Air Vehicle Program at the NASA Glenn Research Center.



*Level of Review*: This material has been technically reviewed by technical management.

This report is available in electronic form at https://www.sti.nasa.gov/ and https://ntrs.nasa.gov/

# High-Temperature Solid Particle Erosion Behavior of an Environmental Barrier Coating

Michael J. Presby
National Aeronautics and Space Administration
Glenn Research Center
Cleveland, Ohio 44315

## Summary

The solid particle erosion (SPE) behavior of a state-of-the-art environmental barrier coating (EBC) was assessed at 1,200 °C, using alumina ($Al_2O_3$) erodent. The effect of particle velocity, particle size, and impingement angle were investigated. Results show that the erosion damage in the EBC is primarily controlled by particle kinetic energy. In addition, the effect of impingement angle demonstrates the contribution of the tangential component of velocity.

## Introduction

Advancements in hot-section materials technology are critical for next-generation gas-turbine engines as the aeronautics industry pushes towards improving thermal and propulsive efficiency while reducing harmful emissions to the environment (Ref. 1). Ceramic matrix composites (CMCs) are revolutionizing the industry because of their high-temperature capability, high strength, toughness, and low density (Refs. 1 and 2). However, silicon-carbide- (SiC-) based CMCs are susceptible to surface recession as a consequence of thermochemical reactions with water vapor, which is a byproduct of combustion (Ref. 2). Environmental barrier coatings (EBCs) were developed to combat this mode of degradation, resulting in enhanced durability and improved life of SiC-based CMC materials and components (Refs. 2 and 3).

Significant advancements in EBC and CMC technology have occurred over the past three decades: the first CMC component with an EBC, a high-pressure turbine shroud, entering service in the LEAP engine designed by CFM International for the Airbus A320neo in 2016 and the Boeing 737 MAX in 2017 (Refs. 2 and 3). Today, advancements continue with the goal of extending EBC-CMC technology to the development and integration of combustor liners, vanes, and blades (Refs. 2 and 3).

In service, EBC-CMC components will experience both thermochemical and thermomechanical modes of degradation. Thermochemical degradation includes water-vapor-induced oxidation and recession and calcium magnesium aluminosilicate (CMAS) attack. The thermomechanical mode includes degradation due to mechanical loading such as fatigue and creep, foreign object damage (FOD), and solid particle erosion (SPE). Ultimately, each of these degradation modes will be operative to varying degrees, and the synergy between them will lead to complex EBC failure modes (Ref. 3).

The objective of this work is to investigate the SPE response of a state-of-the-art EBC to characterize the effect of particle velocity, particle size, and impingement angle. Erosion testing is performed at 1,200 °C (2,192 °F) using alumina ($Al_2O_3$) erodent in a simulated combustion environment.

## Experimental Procedure

The SPE experiments in this work were performed at the NASA Glenn Research Center Erosion Burner Rig Facility. The facility was initially developed to characterize the SPE behavior of thermal barrier coatings (TBCs) in a simulated combustion environment (Refs. 4 to 6) and has recently been used to characterize current and next-generation EBCs and CMCs (Refs. 7 and 8).

## Material System

The EBC system used in this work is proprietary. As a result, the EBC composition, microstructure, and spray parameters cannot be disclosed. The EBC was deposited on a silicon-carbide-fiber-reinforced silicon carbide (SiC/SiC) CMC substrate. The EBC-CMC erosion test samples were machined into 25.4-mm-diameter disks.

## Erosion Facility and Testing

The erosion test facility is a modified NASA Glenn burner rig (Ref. 9) that operates on Jet-A fuel and preheated air. The development of the erosion rig, along with computational fluid dynamics (CFD) modeling and experimental validation have been described in detail elsewhere (Refs. 4 to 6), but an overview is described here briefly. Erodent is delivered using a screw-driven powder feeder (HA 5000F-SA, Hardface Alloys, Inc.): it is injected into the burner chamber, passes through a 19-mm-diameter exit nozzle, and accelerates downstream through a 19-mm-diameter, 305-mm-long unattached duct to the sample (Refs. 4 to 8). A high-temperature, spring-loaded, clamshell fixture fabricated from Inconel® 601 (Special Metals Corporation) is used to hold the sample during testing. A photograph of the burner exit nozzle, the unattached duct, and the sample holder is displayed in Figure 1(a), and a schematic of the burner placed just before the duct is shown in Figure 1(b). The burner rig can be pivoted to heating and cooling positions using a pneumatic actuator and is shown in the cooling position in Figure 1(a). The standoff distance between the duct exit and the center of the sample was set to 30 mm.

Samples were heated to 1,200 °C as measured by an Ircon® Modline® (Fluke Process Instruments) 7.9-μm single-color pyrometer. After reaching the target temperature and letting the temperature stabilize for approximately 5 min, the samples were exposed to $Al_2O_3$ erodent that was fed into the burner at a rate of 2 g/min. Two particle sizes $d$, two particle velocities $v$, and two impingement angles $\alpha$ were used in this study. The overall test matrix is shown in Table I. Three samples were tested at each condition. The particle size $d$ reported in Table I is the mean equivalent spherical diameter that was determined through a particle size distribution analysis. The particle velocities were measured using a double-disk velocimeter that was adapted for use at high temperature (Refs. 7, 8, 10, and 11).

Samples were subject to multiple exposures of 30 s (1 g of erodent), and the sample mass was measured before and after each successive exposure using a scale with precision of 0.01 mg. The steady-state erosion rate was determined from a regression fit in the linear region of the cumulative mass loss versus cumulative mass of erodent curve. For consistency, the regression analysis was performed on the last six data points of each curve.

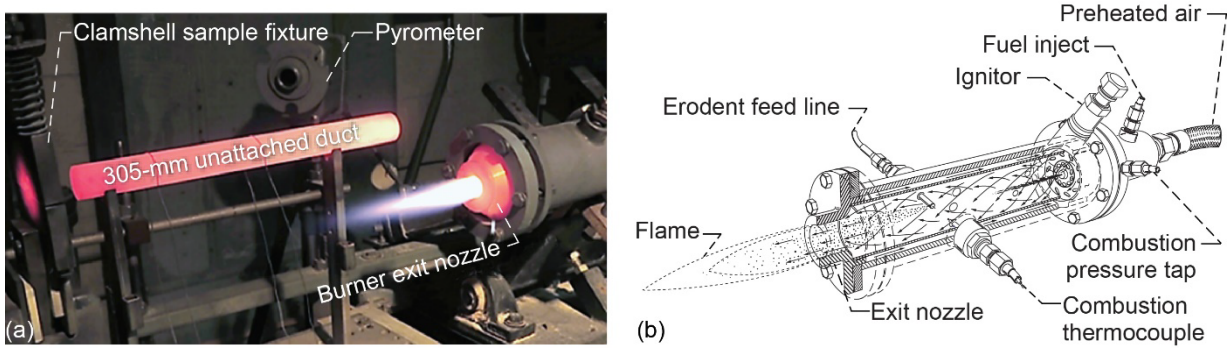


Figure 1.—Erosion test facility burner configuration. (a) Burner exit nozzle, unattached duct, and sample holder (Ref. 7). (b) Burner placed before duct (Refs. 7 and 9).

TABLE I.—TEST MATRIX FOR EBC EROSION BY ALUMINA

| Test condition | Particle size, $d$, μm | Particle velocity, $v$, m/s | Impingement angle, α, deg |
|---|---|---|---|
| 1 | 60 | 100 | 30 |
| 2 | 60 | 100 | 90 |
| 3 | 60 | 135 | 30 |
| 4 | 60 | 135 | 90 |
| 5 | 150 | 100 | 30 |
| 6 | 150 | 100 | 90 |
| 7 | 150 | 135 | 30 |
| 8 | 150 | 135 | 90 |

## Results and Discussion

The erosion rate dependencies are presented for the test conditions shown in Table I. The cumulative mass loss versus cumulative mass of erodent is determined for the different test conditions. The steady-state erosion rate is then assessed with respect to $v$, $d$, and particle kinetic energy $U_k$ for the two different angles α. Finally, the effect of α is further assessed to demonstrate the contribution of the tangential component of particle velocity $v_T$.

### Cumulative Mass Loss Versus Cumulative Mass of Erodent

Exemplary cumulative mass loss $m_l$ versus cumulative mass of erodent $m_e$ curves are shown in Figure 2 for $d$ = 60 μm (Figure 2(a)) and $d$ = 150 μm (Figure 2(b)). The curves exhibit fairly linear behavior throughout the entire 10-g exposure. For a fixed $d$ and α, the cumulative mass loss increases as $v$ increases from 100 to 135 m/s. Likewise, for a fixed $d$ and $v$, the cumulative mass loss increases as α increases from 30° to 90°. On the basis of cumulative mass of erodent, the cumulative mass loss for fixed $v$ and α are similar for $d$ = 60 and 150 μm.

### Steady-State Erosion Rate

The steady-state erosion rate $E$ as a function of $v$ is shown in Figure 3 for $d$ = 60 and 150 μm and α = 30° and 90°. To account for the fact that the cumulative number of particles, and hence the total number of impact events per gram of erodent, is different for $d$ = 60 and 150 μm, $E$ is defined as mass loss per particle impact (mg/impact) as follows:

$$E = \frac{\mathrm{d}\, m_l}{\mathrm{d}\, m_e} m_p \tag{1}$$

where $\mathrm{d}m_l/\mathrm{d}m_e$ is the slope of the linear region (last six data points) of the cumulative mass loss versus cumulative mass of erodent curve and $m_p$ is the mass of an individual particle. The mass of an individual particle was determined using the mean particle size ($d$ = 60 and 150 μm) and density of $Al_2O_3$ (3.95 g/cm$^3$), while approximating the particles to be spheres. Despite only two particle velocities being used in this work, it has been established previously that $E$ follows a power-law dependence with $v$ of the form:

$$E = \phi v^n \tag{2}$$

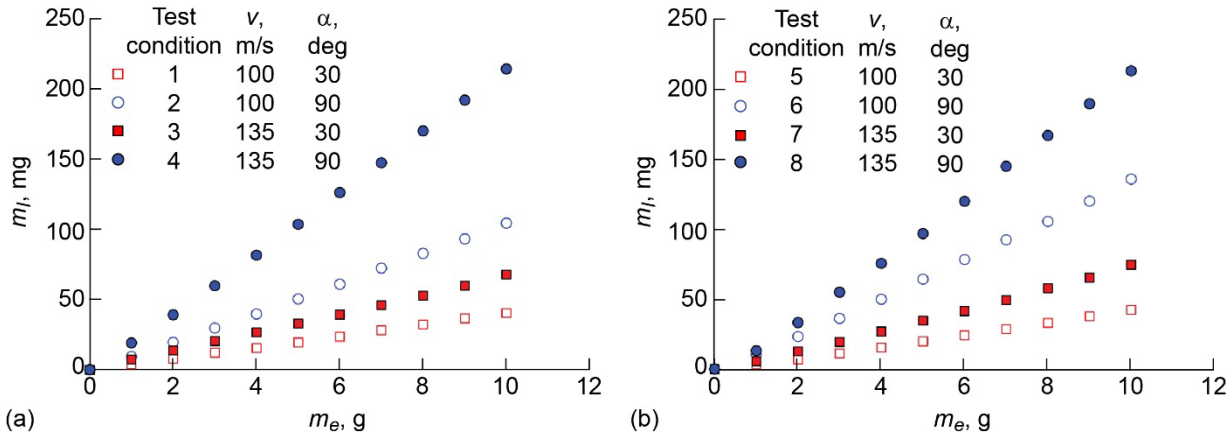


Figure 2.—Cumulative mass loss, $m_l$, versus cumulative mass of erodent, $m_e$, curves for EBC erosion test conditions in Table I by alumina erodent of different particle sizes $d$ with velocities $v$ = 100 and 135 m/s and impingement angles $\alpha$ = 30° and 90°. (a) $d$ = 60 μm. (b) $d$ = 150 μm.

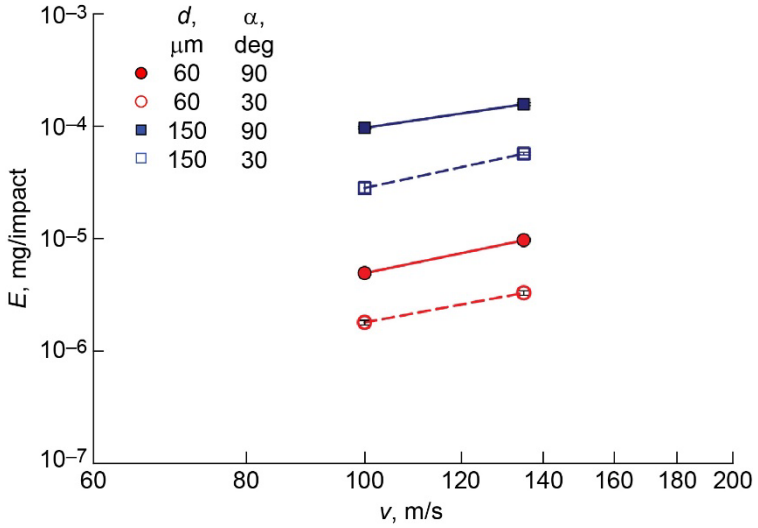


Figure 3.—Steady-state erosion rate $E$ of EBC as function of alumina erodent particle velocity $v$ for particle sizes $d$ = 60 and 150 μm and impingement angles $\alpha$ = 30° and 90°.

where $\phi$ is a constant of proportionality that is a function of target and particle properties, test conditions, and so forth, and $n$ is the velocity exponent (Refs. 11 to 14). Table II displays the values of $\phi$ and $n$ for the data shown in Figure 3. The exponent $n$ varies between 1.62 and 2.36 and is within the range reported by other studies on ceramics and coatings (Refs. 7, 8, and 11 to 20). As shown in Figure 3, $E$ increases with $v$ for a fixed $d$ and $\alpha$. Similarly, $E$ increases as $\alpha$ and $d$ increase for a fixed $v$. For comparison, Figure 4 shows the same data plotted in Figure 3, but with $E$ expressed as mass loss per gram of erodent (mg/g). Although similar trends are observed in Figure 4 as in Figure 3, the effect of increasing $d$ for fixed $v$ and $\alpha$ is not as readily apparent. This is because the erosion rate is dependent upon the damage and material loss associated with the cumulative number of impact events and less dependent on the absolute mass of erodent used.

TABLE II.—CONSTANT OF PROPORTIONALITY ϕ AND VELOCITY EXPONENT *N* FOR THE EROSION OF EBC BY ALUMINA

| Particle size, *d*, μm | Impingement angle, α, deg | Proportionality constant, ϕ | Velocity exponent, *n* |
|---|---|---|---|
| 60 | 30 | $1.69\times10^{-10}$ | 2.01 |
| 60 | 90 | $1.54\times10^{-10}$ | 2.25 |
| 150 | 30 | $5.39\times10^{-10}$ | 2.36 |
| 150 | 90 | $5.60\times10^{-8}$ | 1.62 |

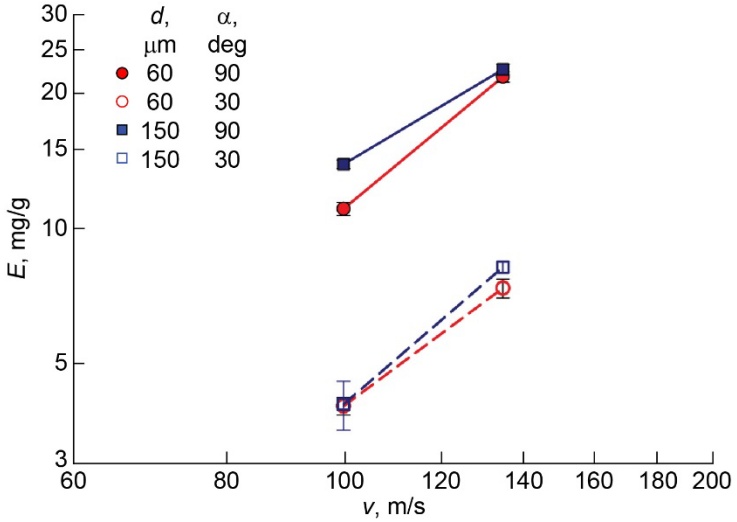


Figure 4.—Steady-state erosion rate *E* of EBC as function of alumina erodent particle velocity *v* for particle sizes *d* = 60 and 150 μm and impingement angles α = 30° and 90°.

Despite the complexity and stochastic nature of the erosion process, the velocity exponents in Table II appear to average out to a value close to 2, suggesting the erosion behavior is directly proportional to particle kinetic energy $U_k$, defined as $U_k = \frac{1}{2} m_p v^2$.

The steady-state erosion rate as a function of particle kinetic energy is shown graphically in Figure 5. A regression analysis yields the following relationship:

$$E = \beta U_k^b \tag{3}$$

where the constant $\beta = 2.20\times10^{-6}$ and exponent $b = 1.04$ for the 90° data set; also, $\beta = 7.80\times10^{-7}$ and $b = 1.02$ for the 30° data set.

For erosion processes controlled by brittle fracture, it has been suggested (Refs. 14 to 17) that the erosion response at oblique impingement angles should be controlled by the normal component of velocity $v_N$, where

$$v_N = v \sin\alpha \tag{4}$$

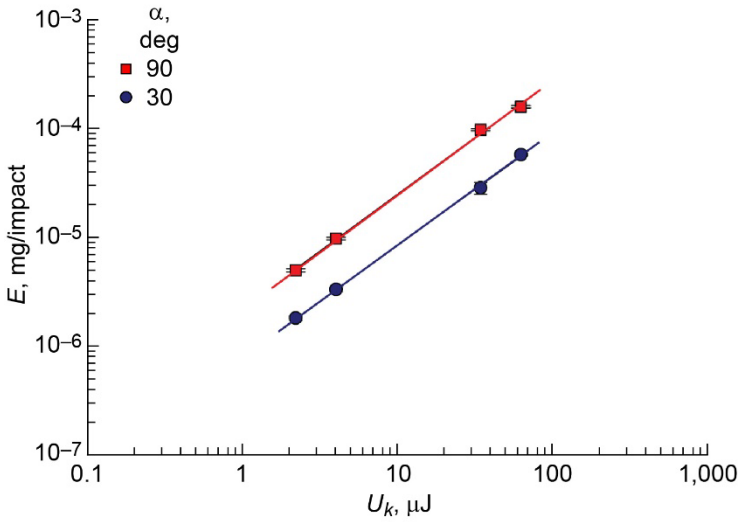


Figure 5.—Steady-state erosion rate $E$ of EBC as function of alumina erodent particle kinetic energy $U_k$ for impingement angles $\alpha$ = 30° and 90°.

However, several studies (Refs. 7, 8, 14 to 18, and 20) on the erosion of brittle materials have shown that the tangential component of velocity $v_T$, defined as

$$v_T = v\cos\alpha \tag{5}$$

contributes to the overall erosion response where the impacting particle slides along the surface, generating wear scars or grooves that are typically associated with a ductile erosion process. To understand the contribution of $v_T$ to the erosion process of the EBC, the erosion data were plotted versus the kinetic energy of the normal component of velocity $U_{k,N}$, which is defined as

$$U_{k,N} = \frac{1}{2} m_p \left(v_N\right)^2 \tag{6}$$

and the result is shown graphically in Figure 6. A regression analysis yields the following:

$$E = \gamma U_{k,N}^b \tag{7}$$

where $\gamma = 2.20\times10^{-6}$ and $b = 1.04$ for the 90° data set, and $\gamma = 3.2310^{-6}$ and $b = 1.02$ for the 30° data set. If there was no contribution from $v_T$ to the erosion process, then the 30° and 90° data sets would be represented by a single regression fit. However, the 30° data set is displaced upward from the 90° data set. The upward displacement of the 30° data set can be quantified by calculating a percent upward displacement parameter (Ref. 14), *PUD*, given as

$$PUD = \frac{E_{30} - E_{90}}{E_{90}} \times 100 \tag{8}$$

where $E_{30}$ and $E_{90}$ are the steady-state erosion rate for 30° and 90°, respectively, at the same $U_{k,N}$. The average *PUD* for the data, shown in Figure 6, is approximately 47 percent.

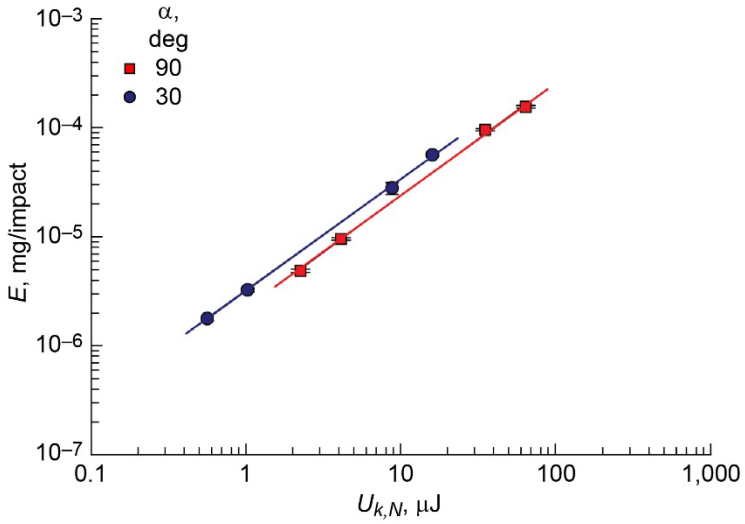


Figure 6.—Steady-state erosion rate $E$ of EBC as function of particle kinetic energy $U_{k,N}$ of normal component of velocity $U_{k,N}$ of alumina erodent for impingement angles $\alpha$ of 30° and 90°.

## Conclusions

Solid particle erosion (SPE) in gas-turbine engines is a complex process and a function of many variables that will change with operating conditions and environment. The target properties, erosion conditions (particle size, shape, velocity, impingement angle, etc.), engine operating conditions (temperature, pressure, etc.), and environment (particle composition) will all play a role in the overall erosion response. As the use of environmental-barrier-coated ceramic-matrix-composite (EBC-CMC) hardware in gas-turbine engines increases, it is important to develop an understanding of the operative erosion mechanisms. Developing a fundamental understanding of the erosion processes in EBC-CMC systems can lead to improved design and fabrication of erosion-resistant materials and to the formulation of appropriate physics-based erosion models.

In this work, the SPE behavior of a state-of-the-art EBC was characterized at 1,200 °C using $Al_2O_3$ erodent. Two particle sizes, $d$ = 60 and 150 μm; two velocities, $v$ = 100 and 135 m/s; and two impingement angles, $\alpha$ = 30° and 90°, were investigated. The steady-state erosion rate $E$ was shown to increase as particle size, particle velocity, and impingement angle increased. Particle kinetic energy was shown to be the controlling variable, where $E \propto U_k^b$ and $b \approx 1$. Finally, the contribution of the tangential component of the impacting particle was assessed. This contribution was quantified using a percent upward displacement value, *PUD*. A *PUD* value of 47 percent was obtained for this EBC system.

## References

1. Zok, F.W.: Ceramic-Matrix Composites Enable Revolutionary Gains in Turbine Engine Efficiency. Am. Ceram. Soc. Bull., vol. 95, no. 5, 2016, pp. 22–28.
2. Lee, Kan N.; and van Roode, Mark: Environmental Barrier Coatings Enhance Performance of SiC/SiC Ceramic Matrix Composites. Am. Ceram. Soc. Bull., vol. 98, no. 3, 2019, pp. 46–53.
3. Lee, Kang N.; Zhu, Dongming; and Lima, Rogerio S.: Perspectives on Environmental Barrier Coatings (EBCs) Manufactured via Air Plasma Spray (APS) on Ceramic Matrix Composites (CMCs): A Tutorial Paper. J. Therm. Spray Technol., vol. 30, 2021, pp. 40–58.

4. Kuczmarski, Maria A.; Miller, Robert A.; and Zhu, Dongming: CFD-Guided Development of Test Rigs for Studying Erosion and Large-Particle Damage of Thermal Barrier Coatings. Model. Simul. Eng., vol. 2011, Article ID 837921, 2011.
5. Miller, Robert A.; Kuczmarski, Maria A.; and Zhu, Dongming: Burner Rig With an Unattached Duct for Evaluating the Erosion Resistance of Thermal Barrier Coatings. NASA/TM—2011-217008, 2011. https://ntrs.nasa.gov
6. Miller, Robert A.; and Kuczmarski, Maria A.: Burner Rig for Small Particle Erosion Testing of Thermal Barrier Coatings. J. Test. Eval., vol. 42, no. 3, 2014.
7. Presby, Michael J.; and Harder, Bryan J.: Solid Particle Erosion of a Plasma Spray—Physical Vapor Deposition Environmental Barrier Coating in a Combustion Environment. Ceram. Int., vol. 47, no. 17, 2021, pp. 24403–24411.
8. Presby, Michael J.: High-Temperature Solid Particle Erosion in a Melt-Infiltrated SiC/SiC Ceramic Matrix Composite. J. Eng. Gas Turbines Power, vol. 143, no. 12, 2021, pp. 121026-1–121026-6.
9. Fox, Dennis S., et al.: Mach 0.3 Burner Rig Facility at the NASA Glenn Materials Research Laboratory. NASA/TM—2011-216986, 2011. https://ntrs.nasa.gov
10. Ruff, A.W.; and Ives, L.K.: Measurement of Solid Particle Velocity in Erosive Wear. Wear, vol. 35, no. 1, 1975, pp. 195–199.
11. Wiederhorn, S.M.; and Hockey, B.J.: Effect of Material Parameters on the Erosion Resistance of Brittle Materials. J. Mater. Sci., vol. 18, 1983, pp. 766–780.
12. Wiederhorn S.M.; and Lawn, B.R.: Strength Degradation of Glass Impacted With Sharp Particles: I, Annealed Surfaces. J. Am. Ceram. Soc., vol. 62, no. 1–2, 1979, pp. 66–70.
13. Marshall, D.B.; Lawn, B.R.; and Evans, A.G.: Elastic/Plastic Indentation Damage in Ceramics: The Lateral Crack System. J. Am. Ceram. Soc., vol. 65, no. 11, 1982, pp. 561–566.
14. Srinivasan, Sreeram; and Scattergood, Ronald O.: R Curve Effects in Solid Particle Erosion of Ceramics. Wear, vol. 142, no. 1, 1991, pp. 115–133.
15. Ritter, J.E.; Rosenfeld, L.; and Jakus, K.: Erosion and Strength Degradation in Alumina. Wear, vol. 111, no. 4, 1986, pp. 335–346.
16. Zhou, Jianren; and Bahadur, Shyam: Erosion Characteristics of Alumina Ceramics at High Temperatures. Wear, vols. 181–183, 1995, pp. 178–188.
17. Routbort, J.L.; Scattergood, R.O.; and Turner, A.P.L.: The Erosion of Reaction-Bonded SiC. Wear, vol. 59, 1980, pp. 363–375.
18. Shin, Dongyun; and Hamed, Awatef: Influence of Micro-Structure on Erosion Resistance of Plasma Sprayed 7YSZ Thermal Barrier Coating Under Gas Turbine Operating Conditions. Wear, vols. 396–397, 2018, pp. 34–47.
19. Cernuschi, F., et al.: Solid Particle Erosion of Thermal Spray and Physical Vapour Deposition Thermal Barrier Coatings. Wear, vol. 271, nos. 11–12, 2011, pp. 2909–2918.
20. Panakarajupally, Ragav P., et al.: Solid Particle Erosion Behavior of Melt-Infiltrated SiC/SiC Ceramic Matrix Composites (CMCs) in a Simulated Turbine Engine Environment. Compos. B Eng., vol. 216, no. 108860, 2021.